iScience

CellPress
OPEN ACCESS

Article

The interplay between SARS-CoV-2 infected airway epithelium and immune cells modulates regulatory/inflammatory signals

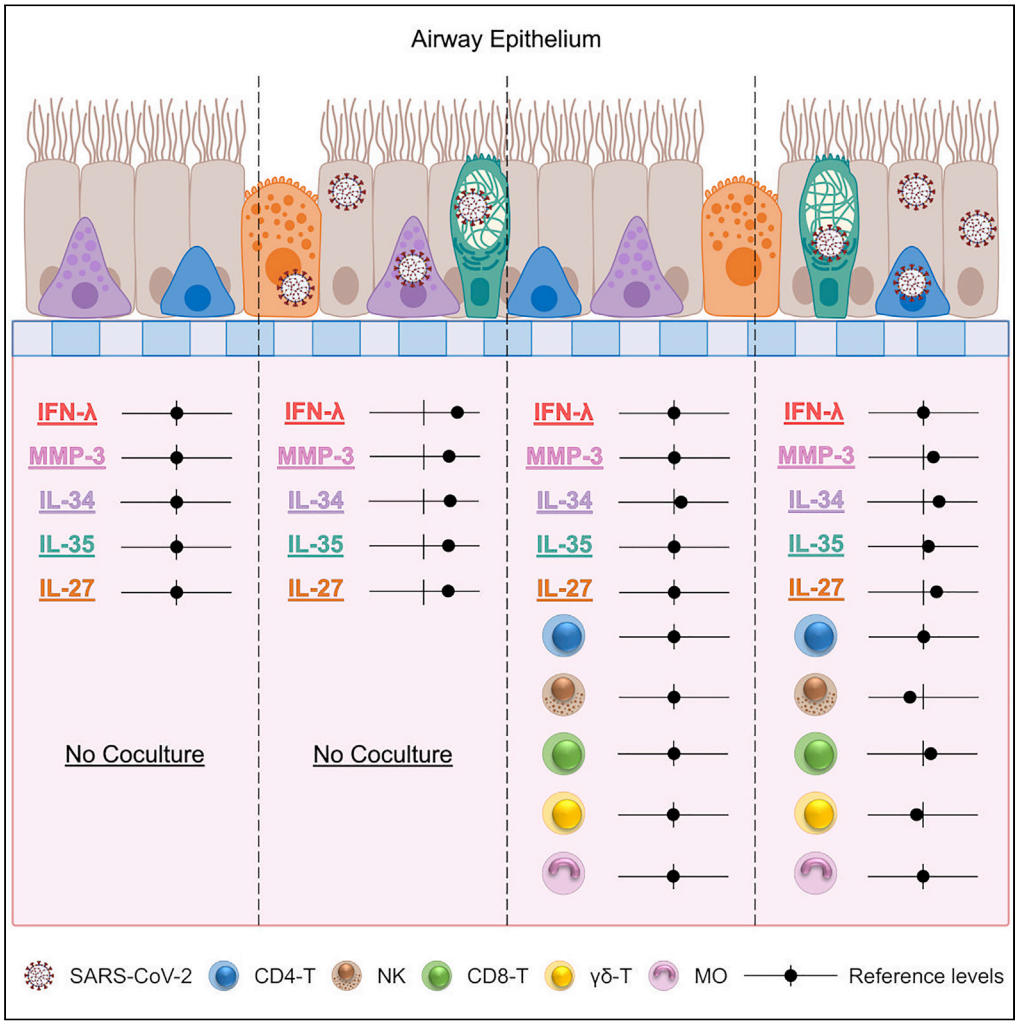

Veronica Bordoni, Giulia Matusali, Davide Mariotti, ..., Maria Rosaria Capobianchi, Giuseppe Ippolito, Chiara Agrati

chiara.agrati@inmi.it

Highlights

HAE as a model to study the cross-talk between infected epithelium and immune cells

Immune cells failed to inhibit SARS-CoV-2 replication

Immune cells dampen the production of several signals induced by SARS-CoV-2 infection

Decrease of NK/γδ T and increase of CD8 T cells in SARS-CoV-2 infected HAE co-culture

Bordoni et al., iScience 25, 103854
February 18, 2022
https://doi.org/10.1016/j.isci.2022.103854

iScience

CellPress
OPEN ACCESS

Article

The interplay between SARS-CoV-2 infected airway epithelium and immune cells modulates regulatory/inflammatory signals

Veronica Bordoni,[1] Giulia Matusali,[1] Davide Mariotti,[1] Manuela Antonioli,[1] Eleonora Cimini,[1] Alessandra Sacchi,[1] Eleonora Tartaglia,[1] Rita Casetti,[1] Germana Grassi,[1] Stefania Notari,[1] Concetta Castilletti,[1] Gian Maria Fimia,[1,2] Maria Rosaria Capobianchi,[1] Giuseppe Ippolito,[1] and Chiara Agrati[1,3,*]

SUMMARY

To assess the cross-talk between immune cells and respiratory tract during SARS-CoV-2 infection, we analyzed the relationships between the inflammatory response induced by SARS-CoV-2 replication and immune cells phenotype in a re-constituted organotypic human airway epithelium (HAE). The results indicated that immune cells failed to inhibit SARS-CoV-2 replication in the HAE model. In contrast, immune cells strongly affected the inflammatory profile induced by SARS-CoV-2 infection, dampening the production of several immunoregulatory/inflammatory signals (e.g., IL-35, IL-27, and IL-34). Moreover, these mediators were found inversely correlated with innate immune cell frequency (NK and γδ T cells) and directly with CD8 T cells. The enriched signals associated with NK and CD8 T cells highlighted the modulation of pathways induced by SARS-CoV-2 infected HAE. These findings are useful to depict the cell-cell communication mechanisms necessary to develop novel therapeutic strategies aimed to promote an effective immune response.

INTRODUCTION

The clinical presentation of SARS-CoV-2 infection ranges from asymptomatic cases to mild upper respiratory tract infection to bilateral pneumonia with acute respiratory distress syndrome (ARDS) and multiple organ failure (Guan et al., 2020; Huang et al., 2020; Zhou et al., 2020). Pathological examination indicates that SARS-CoV-2 targets primarily the airways tract and the lungs (Tian et al., 2020; Xu et al., 2020). COVID-19 infection is characterized by inflammatory infiltrates in the alveolar space and by a systemic inflammatory cytokine storm, suggesting the role of excessive immune response in damaging lung function (Huang et al., 2020; Liao et al., 2020; Song et al., 2020). The inflammatory storm is able to orchestrate pleiotropic activities, resulting in tissue damage, thrombotic events, lymphocytes apoptosis and finally affecting the generation of a balanced and protective immune response (Zhou et al., 2020; Mehta et al., 2020). Induction of interferons appears to be limited in the more severe clinical cases, suggesting an imbalance between protective antiviral and detrimental inflammatory cytokine responses (Blanco-Melo et al., 2020; Hadjadj et al., 2020).

The interplay between epithelial and immune cells during respiratory viral infections is critical in orchestrating and inducing antiviral responses rather than an excessive inflammation. Cytokines and chemokines produced by infected epithelial cells are able to recruit, activate, and coordinate innate and adaptive immune functions. Although a majority of studies focused on the interactions between respiratory epithelial and innate myeloid immune cells, few data are available on respiratory epithelium/lymphocytes cross talk. For example, RSV-infected epithelial cells promote a T cell-independent antibody response, which is important for protection against reinfection (McNamara et al., 2013). Furthermore, the strong interactions between epithelial and immune cells described in nasopharyngeal and bronchial samples from patients with severe COVID-19 are likely to contribute to epithelial cell death (Chua et al., 2020).

Organotypic cell culture of human airway epithelial cells (HAE) sustains SARS-CoV-2 replication and has been used to characterize SARS-CoV-2 cell tropism, replication, and pathogenesis (Zhou et al., 2020; Ravindra et al., 2021; Zhou et al., 2020; Hao et al., 2020; Pizzorno et al., 2020).

[1]National Institute for Infectious Diseases Lazzaro Spallanzani-IRCCS, Via Portuense, 292, Rome 00149, Italy

[2]Department of Molecular Medicine, University of Rome "Sapienza", Rome, Italy

[3]Lead contact

*Correspondence: chiara.agrati@inmi.it

https://doi.org/10.1016/j.isci.2022.103854

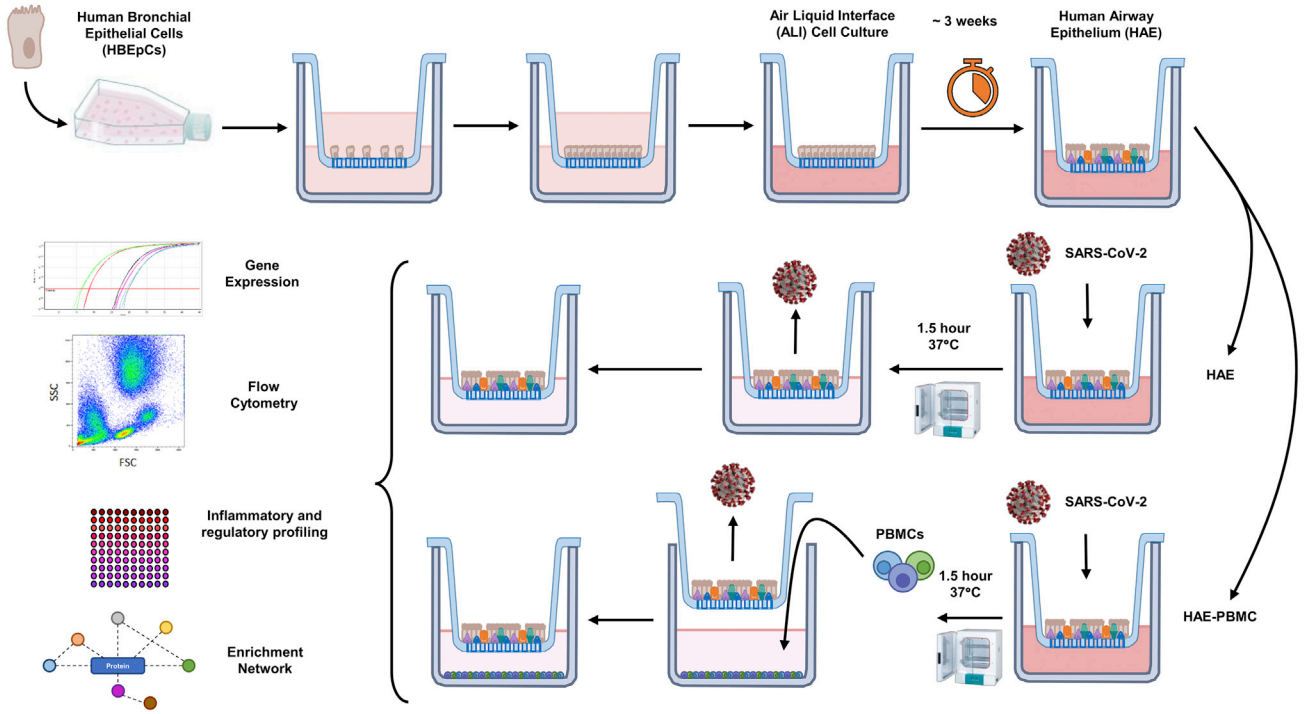

Figure 1. Experimental model and design

Human bronchial epithelial cells were seeded onto the permeable membrane of a cell culture insert and once confluence was reached, the cells were subjected to "airlift," where the medium was supplied only to the basal chamber, driving differentiation toward a mucociliary phenotype. After 21 days, the organotypic human airway epithelial (HAE) culture were infected (or not) with SARS-CoV-2 and co-cultured in the absence (HAE) or in the presence of healthy Peripheral Blood Mononuclear Cells (HAE-PBMC) in the lower chamber. Infected cultures were collected for gene expression analysis, flow cytometry, inflammatory/regulatory soluble factors profile at 6-days postinfection. Four independent experiments using immune cells isolated from four different healthy donors were performed in duplicate.

Here, to better understand the interplay between immune cells and the epithelial tissue during SARS-CoV-2 replication, we analyzed the impact of SARS-CoV-2 infection on inflammatory response and immune cells phenotype in an organotypic co-culture of human bronchial epithelium and immune cells model.

RESULTS

Co-culture of SARS-CoV-2 infected airway epithelium with immune cells: the experimental model

To investigate the cross talk between SARS-CoV-2-infected human airway epithelium (HAE) and the immune cells, we set up a co-culture model. Specifically, we cultured primary Human Bronchial Epithelial Cells at an air-liquid interface for 21 days and then challenged the apical surface of the epithelium with SARS-CoV-2. Soon after the removal of viral inoculum, the HAE was co-cultured with peripheral blood mononuclear cells (HAE-PBMC). The characterization of viral replication and inflammation profile, as well as the modulation of both innate and adaptive immune subsets (NK, monocytes, γδ T cells, CD4 and CD8 T cells) were performed after 6 days in SARS-CoV-2 infected or not infected HAE and HAE-PBMC. The enriched network and signaling pathways were also evaluated (Figure 1).

Human airway epithelium-peripheral blood mononuclear cells co-culture sustains SARS-CoV-2 replication and induces the interferon response

The ability of airway epithelium to sustain SARS-CoV-2 replication and the impact of immune cells co-culture were analyzed. SARS-CoV-2 replication was measured at two and six days postinfection (p.i.) comparing viral RNA levels released by or associated with epithelial cells, as well as by measuring the infective titers of the viral particles shed to the apical side of the HAE culture model. In HAE, an increase

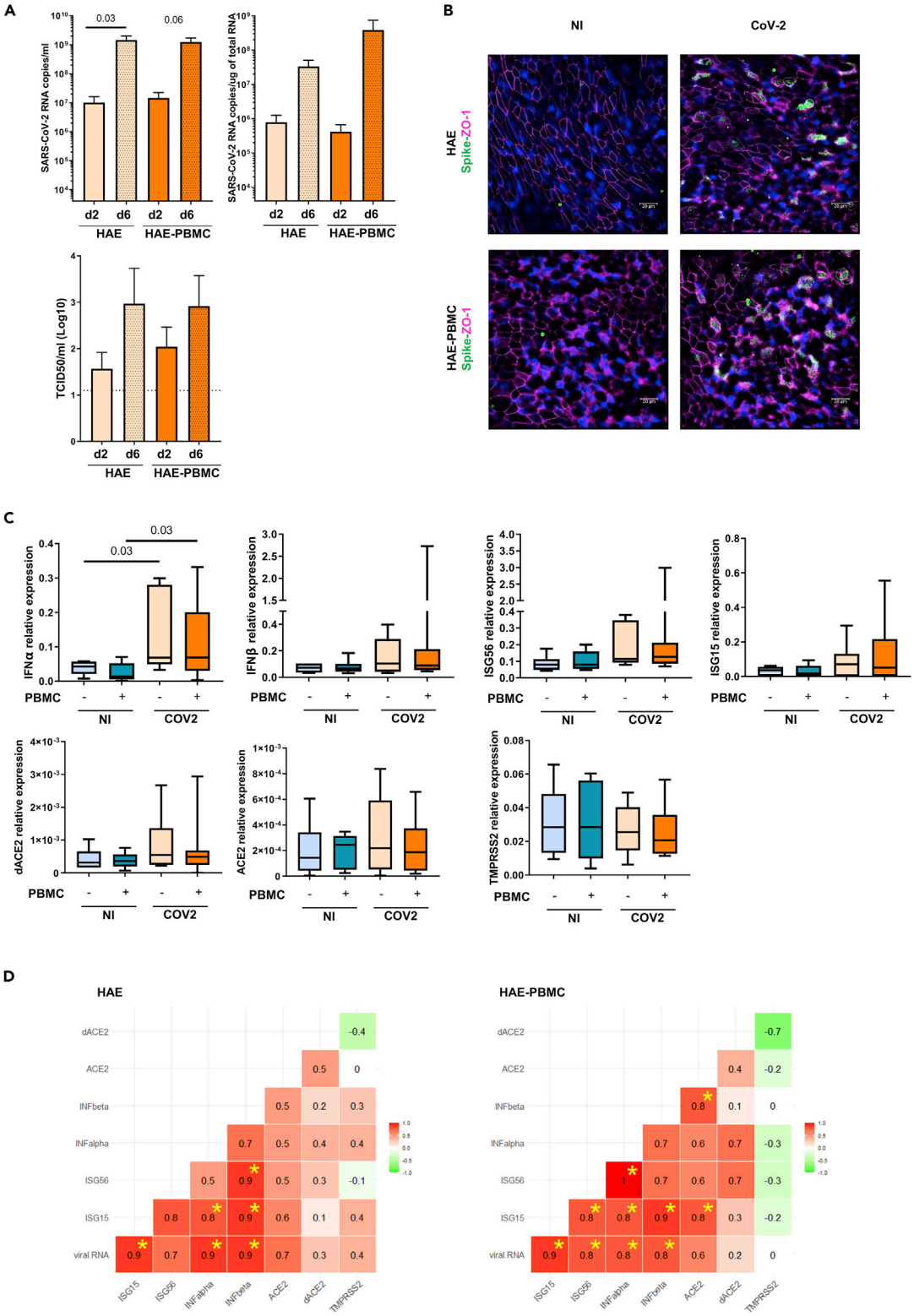
A
SARS-CoV-2 RNA copies/ml
0.03
0.06
d2
d6
d2
d6
HAE
HAE-PBMC
SARS-CoV-2 RNA copies/ug of total RNA
TCID50/ml (Log10)
B
NI
CoV-2
HAE
Spike-ZO-1
HAE-PBMC
Spike-ZO-1
C
IFNα relative expression
IFNβ relative expression
ISG56 relative expression
ISG15 relative expression
dACE2 relative expression
ACE2 relative expression
TMPRSS2 relative expression
PBMC
NI
COV2
D
HAE
HAE-PBMC
dACE2
ACE2
INFbeta
INFalpha
ISG56
ISG15
viral.RNA
TMPRSS2

Figure 2. HAE-PBMC co-culture sustains SARS-CoV-2 replication and induces the IFN response

(A) Replicative dynamics of SARS-CoV-2 in HAE and HAE-PBMC in terms of released and cell-associated viral RNA and released viral particles infectious titer (TCID50) at two and 6dpi (n = 4 independent experiments in biological duplicate). Data are shown as mean + SEM Friedman test with Dunn's post-test addressed the statistical differences. p values are indicated on the graphs.

(B) Representative immunofluorescence analysis of not infected (NI) and SARS-CoV-2-infected HAE and HAE-PBMC (n = 4). Cells were stained with anti-ZO-1 (purple) and anti-spike (green) antibodies. Thunder images were taken at a magnification of 63X. Nuclei were stained with DAPI (blue). Scale bars = 20 μm.

(C) The gene expression analysis of IFN-α, IFN-β, ISGs, ACE, and dACE2 was performed in NI and in SARS-CoV-2 HAE, in the absence (−) or presence (+) of PBMC (n = 4). Data are shown as Box and Whiskers graphs. The Wilcoxon matched-pairs signed rank test was used for group's comparison. . p values are indicated on the graphs.

(D) Correlation matrices across IFN-α, IFN-β, ISG15, ISG56, ACE2, and dACE2 gene expression from HAE and HAE-PBMC co-cultures are shown (n = 4). The significant correlations (<0.05) are indicated with an asterisk. Spearman correlation coefficients are reported.

in released and cell-associated SARS-CoV-2 RNA levels was detected along the culture and no effect of PBMC on viral replication was noticed (Figure 2A). The same profile was observed when measuring the infectious titer (TCID50) of viral particles released by HAE or HAE-PBMC (Figure 2A). In this model, SARS-CoV-2 did not infect PBMC in the lower chamber (data not shown). SARS-CoV-2 infection of HAE and HAE-PBMC was also verified by immunofluorescence for the viral Spike protein, as reported in Figure 2B.

We then focused on the role of immune cells in modulating the antiviral response triggered by SARS-CoV-2 infection of the airway epithelium. The gene expression levels of IFN-α increased after SARS-CoV-2 infection both in HAE and in HAE-PBMC (Figure 2C). The expression of IFN-β, IFN-stimulated genes (ISG15 and ISG56), as well as the truncated form of ACE2, known to have an ISG function (Onabajo et al., 2020), showed a slight increase, although they did not reach the statistical significance (Figure 2C). Furthermore, SARS-CoV-2 infection did not change the gene expression levels of the two main viral entry factors (Figure 2C), namely ACE2 and TMPRSS2 (Hoffmann et al., 2020).

Correlation matrix analysis showed a coordinate IFNs response in HAE culture where viral RNA directly correlates with ISG15, IFN-α, and IFN-β; ISG15 correlated with IFNs and ISG56 with IFN-β (Figure 2D), suggesting the activation of IFN signaling by viral replication. In the presence of PBMC, these correlations seemed to be even stronger and new ones appeared ISG15 correlated with ISG56 and ACE2, ISG56 correlated with viral RNA and, finally, ACE2 correlated with IFN-β. These results suggested that viral replication in the HAE model induced a Type I-IFN signaling independently from the presence of immune cells.

Immune cells modulate the inflammatory response induced by SARS-CoV-2 infection

To evaluate the impact of immune cells on the inflammatory profile induced by SARS-CoV-2 infection, we quantified 36 key biomarkers, belonging to the TNF superfamily proteins, IFN family proteins, regulatory cytokines, and Matrix metalloproteinases (MMPs) in SARS-CoV-2 infected HAE-PBMC. PCA analysis was, therefore, performed in order to identify the major trends inherent to the inflammatory profile. Unsupervised PCA of 36 soluble mediators seemed more efficient at segregating HAE cultures on the basis of the presence of immune cells than on the basis of infection. As showed in Figure 3A: not infected and SARS-CoV-2 infected HAE cultures (blue and red points, respectively) are grouped on the third and fourth quadrants of score plot, while not infected and infected HAE-PBMC are grouped on the opposite (first and second) quadrants (purple and green points), suggesting that the immune cells strongly shape the inflammatory response. The quantification of all the mediators in SARS-CoV-2 infected HAE and in HAE-PBMC are shown in Table 1. In the absence of PBMC, 33/36 cytokines screened showed a slight increase after SARS-CoV-2 infection (Table 1). Of note, the presence of immune cells significantly dampened the infection-induced cytokine production of 10 mediators (highlighted in bold, Table 1). Specifically, in infected HAE-PBMC, the immune cells reduced: (i) cytokines involved in IFN responses (IFN-β and IFN-λ2); (ii) matrix metalloproteinase (MMP3); (iii) immunoregulatory cytokines, IL-27, IL-35, IL-34, and sTNFR1; (iv) sCD30/TNFRSF8, gp130/sIL6RB, and IL-32, involved in the inflammatory response (Figure 3B).

SARS-CoV-2 infection of human airway epithelium-peripheral blood mononuclear cell co-culture modulates immune cell frequency

To verify if SARS-CoV-2 infected HAE may modulate PBMC phenotype we performed a multiparametric flow cytometry analysis of co-cultured PBMCs, focusing on NK cells (CD56 dim, bright, and negative

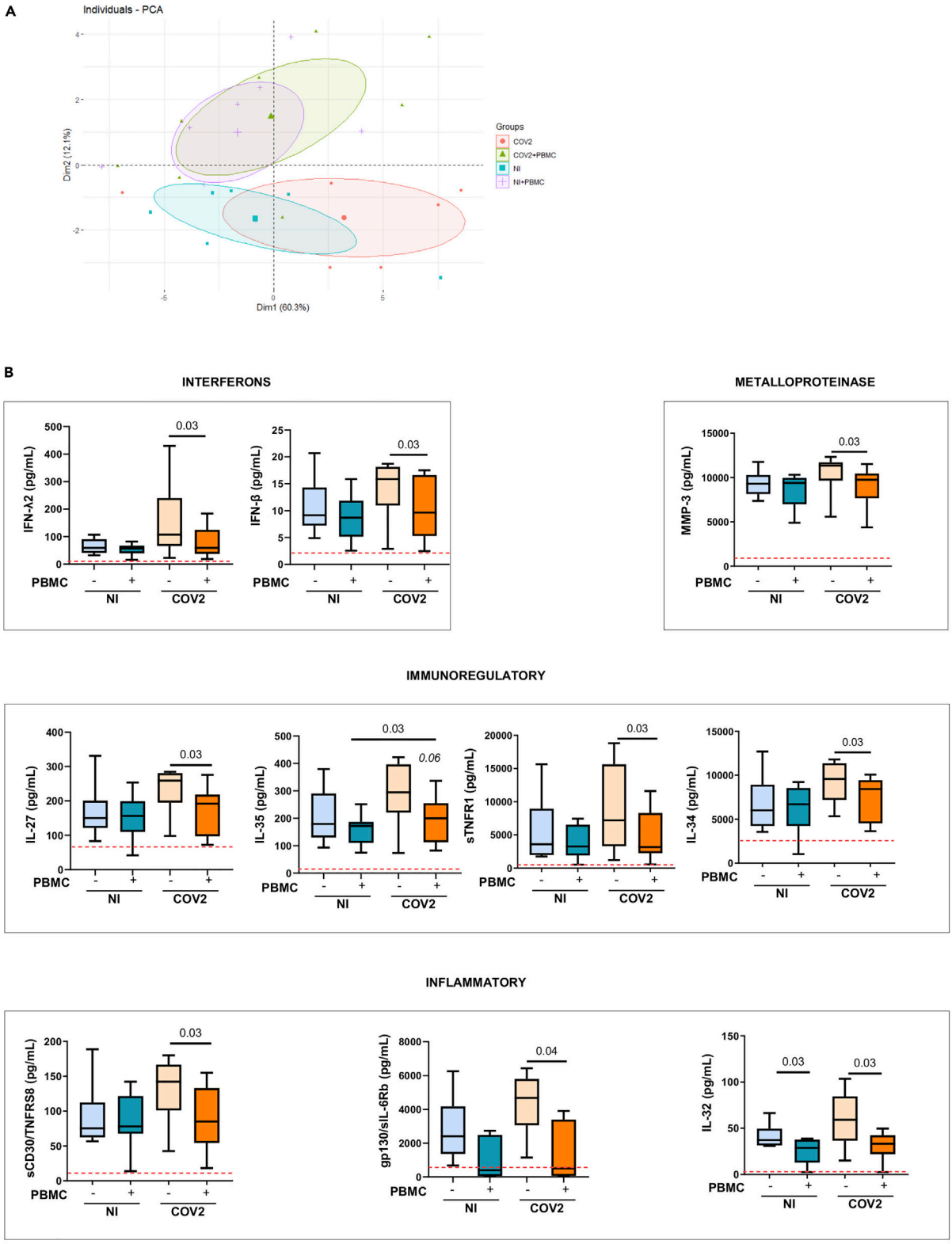
A
Individuals - PCA
Dim2 (12.1%)
Dim1 (60.3%)
Groups
COV2
COV2+PBMC
NI
NI+PBMC
B
INTERFERONS
METALLOPROTEINASE
IFN-λ2 (pg/mL)
IFN-β (pg/mL)
MMP-3 (pg/mL)
IMMUNOREGULATORY
IL-27 (pg/mL)
IL-35 (pg/mL)
sTNFR1 (pg/mL)
IL-34 (pg/mL)
INFLAMMATORY
sCD30/TNFRS8 (pg/mL)
gp130/sIL-6Rb (pg/mL)
IL-32 (pg/mL)
PBMC
NI
COV2
0.03
0.04
0.06

Figure 3. Immune cells modulate the inflammatory profile induced by SARS-CoV-2 infection in HAE-PBMC co-cultures

(A) Principal Component Analysis of the soluble mediators (measured by immunoassay) in HAE and HAE-PBMC co-cultures; Score plot of not infected (NI) HAE and HAE-PBMC are marked, respectively, in blue and purple colors; Score plot SARS-CoV-2 infected HAE and HAE-PBMC are marked, respectively, in red and green colors. Confidence ellipses are drawn to better appreciate differences between groups (n = 4).

(B) Soluble mediators significantly modulated by PBMC in SARS-CoV-2 infected HAE-PBMC (n = 4); results are shown as Box and Whiskers Graphs. Dashed lines indicate the soluble mediator's levels released by PBMC alone. The Wilcoxon matched-pairs signed-rank test was used for group's comparison. p values are indicated on the graphs.

subsets), γδ T cells, monocytes, and adaptive CD4 and CD8 T cells. The results showed a significant decrease of innate cells (CD56 + bright and γδ T cells) and a weak increase of $CD8^+$ T cells between not infected and SARS-CoV-2 infected HAE-PBMC. Of note, the frequency of CD8 T cells was positively correlated with SARS-CoV-2 RNA ($r = 0.78$, $p = 0.02$). No significant differences were observed when looking at $CD16^+$ and CD16 negative monocytes and CD4 T cells (Figure 4).

SARS-CoV-2 infection modulates the soluble mediator's network associated with immune cell subsets in human airway epithelium-peripheral blood mononuclear cell co-cultures

To define possible associations among the immunological parameters and the inflammatory profile in not infected and SARS-CoV-2 infected HAE-PBMC, we performed a correlation matrix among the (36 + 8) continuous variables and build a protein-protein network using Cytoscape (STRING App).

The correlation matrix highlighted that SARS-CoV-2 infection of HAE-PBMC deeply changed the association between soluble factors and lymphomonocytes subsets. The four hierarchical clusters identified in HAE-PBMC were modified by SARS-CoV-2 infection (Figure 5A), where a more consistent group of inflammatory/regulatory mediators was observed (Figure 5A). In not infected co-cultures, the soluble mediators were negatively correlated to NK cells (mainly CD56dim subset) and γδ T cells (Figure 5A green boxes and Figure 5B blue circles), and positively to CD8 T cells (Figure 5A red box, and Figure 5B blue circles). Differently, in SARS-CoV-2 infected co-cultures, the negative associations with NK cells were strongly reduced (Figure 5A green box and Figure 5B, orange circle) while the positive associations with CD8 T cells increased (Figure 5A red box and Figure 5B, orange circles). Furthermore, during the interplay with SARS-CoV-2 infected epithelium, several inflammatory mediators underwent new associations with immune cells (Figures 5A and 5B). Specifically: (i) IFN-α2, IFN-λ2, IFN-λ1, IL-12p40, IL-20, IL-26, IL-35, and osteocalcin are positively associated with CD8 T cells; (ii) IL-10, IL-27 and IL-34 are negatively related to NK CD56bright during infection; and (iii) IFN-α2, IL-35, and MMP3 are negatively associated with γδ T cells. Moreover, PTX3 during infection is negatively correlated to CD4 T cells frequency.

Collectively, these data showed that in SARS-CoV-2 infected HAE-PBMC co-cultures, five of 10 soluble mediators that were modulated by the presence of immune cells, resulted correlated to CD8 T cells, NK-bright and γδ T cells in these ways: IFN-λ, as well as IL-35, were directly correlated with CD8 T cells frequency; MMP3 as well as IL-35 inversely correlated with γδ T cells frequency; IL-27 as well as IL-34 inversely correlated with NK CD56 bright frequency.

In order to explore the enrichment of biological pathways resulting from inflammatory profile and NK cells subset association, we performed STRING Enrichment analysis, grouping soluble factors based on their association with specific lymphomonocytes subset, in the presence or absence of SARS-CoV-2 infection. In SARS-CoV-2 infected HAE-PBMC, the pathways associated with NK-dim cells subsets were profoundly affected, losing most of the associations found in the uninfected conditions (Figure 5C). Interestingly, during SARS-CoV-2 infection, the CD8 T cells subset was associated with the RIG-I pathway.

DISCUSSION

Epithelial cells that span the length of the respiratory tract respond to viral infection by producing soluble mediators that communicate with immune cells to activate and regulate the antiviral response. Organotypic cell culture of human airway epithelial cells (HAE) has been successfully used to isolate SARS-CoV-2 and developed to widely characterize SARS-CoV-2 cell tropism, replication, and pathogenesis (Zhu et al., 2020a; Ravindra et al., 2021; Zhu et al., 2020b; Hao et al., 2020; Pizzorno et al., 2020). However, the cross-talk between immune cells and the infected HAE during SARS-CoV-2 infection has not yet been

Table 1. Quantification of soluble mediators released in SARS-CoV-2 infected HAE co-cultured in presence (+)/absence (–) of PBMC

	Not infected [median pg/mL (IQR)]		SARS-COV-2 [median pg/mL (IQR)]	
Soluble mediators	PBMC –	+	–	+
TNFSF13	77483 (45696–109333)	127025 (62742–172721)	94216 (55066–110437)	118439 (62538–203175)
TNFSF13B	3112 (2901–3735)	3989 (3380–4914)	4562 (3767–4661)	4461 (3486–5183)
TNFRSF8	**75.3 (62.4–112.5)**	**78.1 (67.6–121.6)**	**142.3 (101.1–166.7)**	**85 (54.2–133.1)**
sCD163	6120 (2363–18102)	21422 (2814–32276)	14536 (4452–31509)	28416 (5157–39125)
Chitinase 3-like 1	1671 (1165–2445)	1728 (1391–4669)	3614 (2427–4801)	3122 (1564–5517)
gp130	**2408 (1362–4180)**	**403.2 (49.4–2484)**	**4678 (3061–5801)**	**511.1 (63.7–3392)**
IFNa2	47.6 (35.8–76.9)	44.9 (31.1–52.5)	70.5 (49.7–99.2)	48.1 (32.4–67.4)
IFNb	**9.2 (7.2–14.3)**	**9.3 (6.4–10.4)**	**15.9 (11–18.2)**	**10.1 (6.6–15.2)**
IFNg	37.2 (24.8–61.3)	30.4 (24.8–49.5)	67.5 (37.1–73.1)	29.7 (21.2–61.3)
IL-2	24.8 (18.1–38.8)	27.6 (24.3–56.7)	37.3 (27–53.4)	31 (21.7–89)
sIL-6Ra	44 (20–262.1)	20 (20–168.2)	63.6 (19.7–294.3)	20 (20–201.9)
IL-8	11724 (4993–25370)	11724 (11724–30956)	11724 (9387–37366)	11724 (11724–30956)
IL-10	1.9 (1.9–26.9)	1.9 (1.9–17.6)	29.2 (15–34.5)	1.9 (1.9–24.7)
IL-11	755.9 (503.4–1772)	501.4 (189.5–840.4)	1441 (954.9–1885)	455.9 (219–1518)
IL-12p40	66.8 (51.3–121.9)	62.7 (41.9–78.4)	110.1 (75.5–152.7)	64.6 (42.2–107.6)
IL-12p70	0.7 (0.5–1.1)	0.5 (0.4–1.3)	1.3 (0.5–2.4)	0.7 (0.5–1.8)
IL-19	172.1 (111.8–254.1)	151.6 (93–189.2)	208.1 (172.5–269.2)	153.1 (64–190.1)
IL-20	112.1 (46.8–182.3)	93.9 (65.6–117.5)	143.8 (94.3–262.2)	102.6 (57.2–181)
IL-22	150.3 (135.6–236.1)	184.8 (159.9–239.2)	286.1 (214.1–345.3)	229.9 (140.6–283)
IL-26	942.2 (753.9–1390)	1331 (728.3–1462)	1752 (1270–1957)	1438 (745.2–1883)
IL-27	**150.2 (121.6–200.9)**	**156.6 (110.3–199.2)**	**259 (195.2–280.9)**	**192 (97–218.5)**
IFN-L2	**58.8 (40.7–90.7)**	**56.4 (38.9–66.8)**	**107.3 (65.9–240.4)**	**58.9 (37.2–124.3)**
IFN-L1	128.6 (106.6–196.1)	114.7 (78.3–133.6)	207.6 (154.8–252.6)	121.5 (88.4–207.5)
IL-32	**37.2 (31.5–49.5)**	**28.7 (12.8–37.7)**	**59.1 (36.5–84.6)**	**33.2 (22–42.5)**
IL-34	**6008 (4228–8936)**	**6712 (4229–8540)**	**9587 (7203–11368)**	**8426 (4532–9449)**
IL-35	**179.3 (130.2–290.6)**	**172.1 (110.8–186.9)**	**294.9 (220.8–396.8)**	**200 (112.7–255.3)**
TNFSF14	33 (26–53.6)	42.9 (33.6–60.2)	71.6 (46.7–86.4)	54.2 (29.1–73.2)
MMP-1	2084 (1103–3683)	1922 (1167–2728)	2817 (1857–4179)	1849 (1129–2458)
MMP-2	23857 (6142–50637)	8230 (4656–13600)	23362 (9398–50483)	8510 (5686–21247)
MMP-3	**9303 (8148–10293)**	**9388 (6995–9973)**	**11347 (9651–11719)**	**9762 (7665–10456)**
BGLAP	621.3 (424–967.9)	577.4 (396.7–674.9)	909.2 (658.3–1237)	588.4 (383.5–872.8)
OPN	46.2 (34.9–70.8)	628.5 (52.8–3813)	46.2 (46.2–55.9)	419.4 (95.7–9569)
Pentraxin-3	1087 (567.4–2569)	3311 (2008–4393)	2005 (1339–3079)	3923 (1923–4988)
sTNF-R1	**3604 (1990–8959)**	**3278 (1931–6536)**	**7214 (3303–15628)**	**3178 (2269–8308)**
sTNF-R2	86.8 (70.7–116.6)	251.6 (134.6–577)	148.2 (106.3–164.2)	288.1 (125.9–617.9)
TNFSF12	4.2 (3–31.7)	40.1 (14.6–78.5)	24.1 (14.2–35.4)	42.1 (7–102.7)

In bold are indicated the soluble mediators significantly modulated by PBMC during SARS-CoV-2 infection.

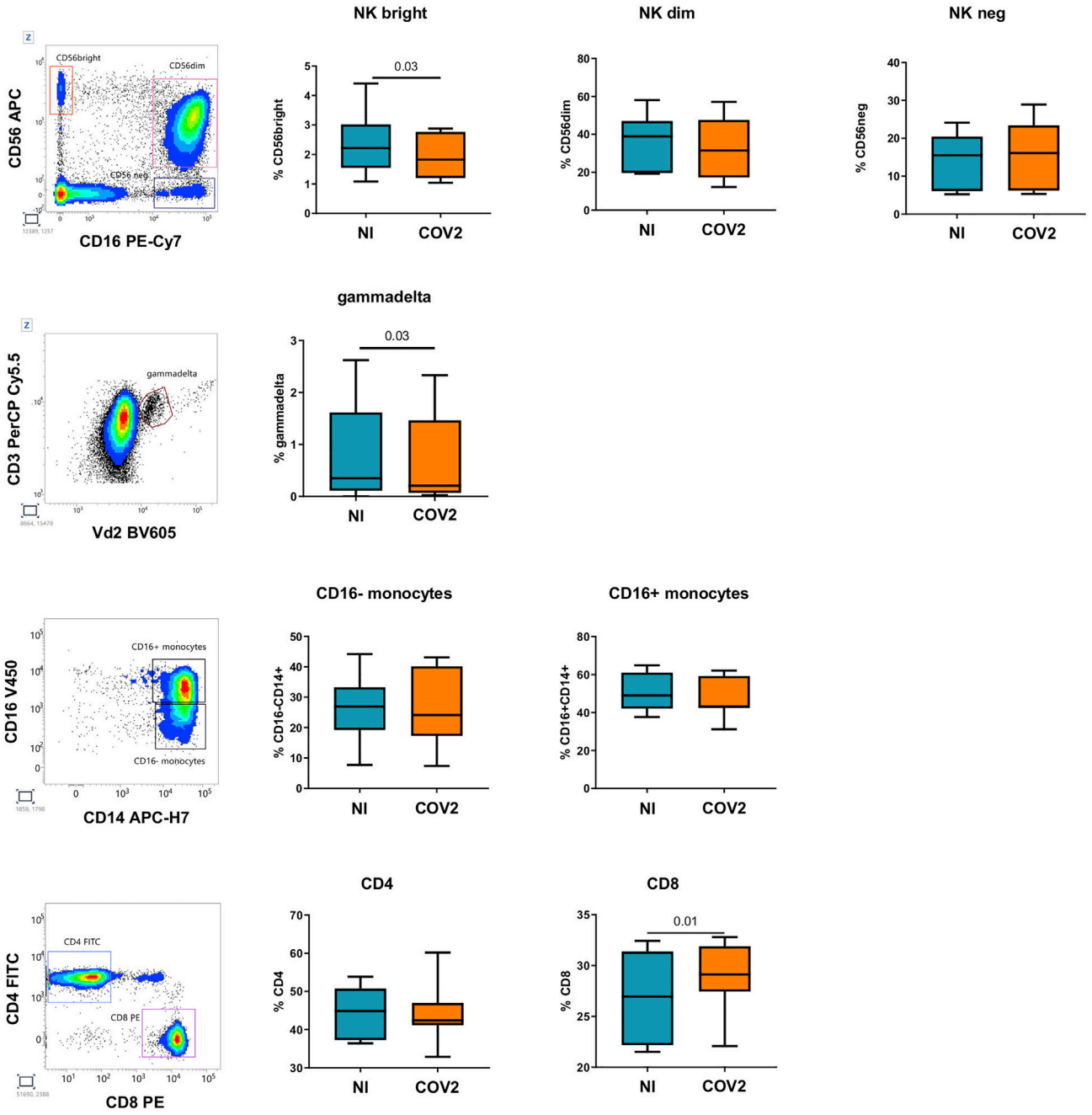

Figure 4. SARS-CoV-2 infection of HAE-PBMC co-cultures modulates immune cell frequency

Representative flow cytometry plots of NK cells, γδ T cells, $CD16^{+}$ and $CD16^{-}$monocytes, CD4 and CD8 T cells frequency after 6 days of co-cultures with SARS-CoV-2 infected HAE (n = 4). Results are shown as Box and Whiskers Graphs. Wilcoxon matched-pairs signed-rank test was used for groups comparison. p values are indicated on the graphs.

investigated. The strength of this article is, therefore, the description of the epithelial-immune cell cross-talk during SARS-CoV-2 infection using an airway epithelial and immune cell co-culture system. Results showed that the immune cells modulate the production of immunoregulatory/inflammatory signals (e.g., IL-35, IL-27, and IL-34) from SARS-CoV-2 infected HAE. These mediators were found inversely correlated with innate cells (NK and γδ T cells) and directly with CD8 T cells, highlighting the strict interplay between immune cells and infected epithelium.

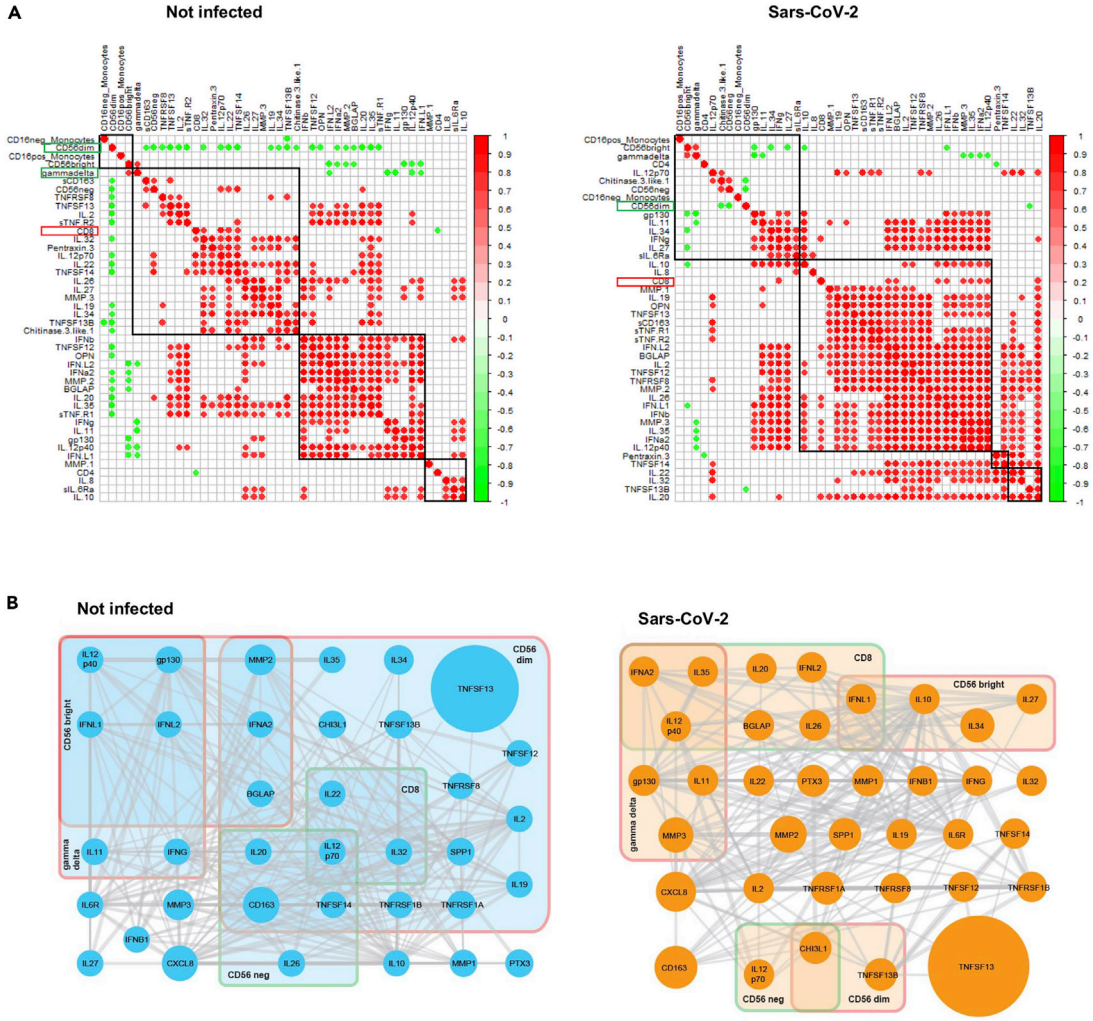
A
Not infected
Sars-CoV-2
B
Not infected
Sars-CoV-2
CD56 bright
CD56 dim
CD56 neg
CD8
gamma delta
C
KEGG pathways
Toll−like receptor signaling pathway
Th17 cell differentiation
RIG−I−like receptor signaling pathway
Rheumatoid arthritis
Proteoglycans in cancer
NF−kappa B signaling pathway
Kaposi's sarcoma−associated herpesvirus infection
Jak−STAT signaling pathway
Intestinal immune network for IgA production
Inflammatory bowel disease (IBD)
Herpes simplex infection
Fluid shear stress and atherosclerosis
Cytokine−cytokine receptor interaction
Chagas disease (American trypanosomiasis)
Autoimmune thyroid disease
Amyotrophic lateral sclerosis (ALS)
Allograft rejection
SARS-Cov-2
cytokines
2.5
5.0
7.5
10.0
12.5
-log FDR
10.0
7.5
5.0
2.5

Figure 5. Inflammatory soluble mediator's network associated with distinct immune cell subsets in SARS-CoV-2 infected HAE-PBMC co-cultures
Correlation between soluble inflammatory mediators and immune cell subsets is not infected (NI, left panel) and SARS-CoV-2 infected HAE-PBMC co-cultures (right panel), (n = 4). The figure shows a Spearman correlation matrix for 36 soluble mediators and NK cells, γδ T cells, $CD16^+$ and CD16-monocytes, CD4 and CD8 T cells frequency. Only statistically significant ($p < 0.05$) parameters are shown: red = positive correlation, green = negative correlation.
(B) Network analysis of soluble inflammatory mediators of HAE-PBMC co-cultures is not infected (NI, left panel) or SARS-Cov-2 infected HAE (right panel), (n = 4). Soluble factors were grouped based on the positive (green boxes) or negative (red boxes) correlation with PBMC subsets. The size of each node represents the concentration expressed in pg/mL (range, not infected: 0.75–1,18 × 105; SARS-COV-2: 1–1,32 × 105 pg/mL).
(C) Bubble plot representation of KEGG-pathways enrichment analysis performed for each of reported PBMC subsets considering associations with soluble factors; only FDR-value<0.05 has been taken into account. The size of each bubble represents the number of soluble factors for the indicated pathway, gradient coloring expresses the statistical significance of the pathway reported as -log FDR-value.

SARS-CoV-2 replicates efficiently in HAE cultured in an airway-liquid interface culture inducing the IFN response, as shown by the direct correlation between viral RNA and ISGs; moreover, the presence of immune cells did not affect viral replication nor antiviral response. Differently from other observations (Chua et al., 2020; Nawijn and Timens, 2020), we did not observe a significant change in the ACE2 and TMPRRS expression probably owing to the high variability of their expression in a pluristratified airway epithelium. Nevertheless, the correlation between ISG15, ISG56, and ACE2 observed only in HAE-PBMC may suggest a possible enhancement in ISG coordination. Interestingly, a recent work demonstrates a crucial role of ISG15 in the MDA5-mediated antiviral response, representing a key immune evasion mechanism of SARS-CoV-2 (Chua et al., 2020).

Cytokines are crucial in the cell-cell communication processes and in shaping the host responses to SARS-CoV-2 infection. Principal component analysis revealed that the presence of immune cells discriminates the inflammatory/regulatory profile in SARS-CoV-2-infected HAE. SARS-CoV-2 infection of HAE induces the release of a wide profile of inflammatory/regulatory soluble mediators. Intriguingly, immune cells significantly reduced the levels of 10 SARS-CoV-2 induced cytokines. Specifically, in SARS-CoV-2 infected HAE-PBMC, the immune cells production of IFNs, MMPs (able to influence the inflammation processes), immunoregulatory cytokines (IL-27, IL-34, IL-35, and sTNFR1) and the inflammatory cytokines (sCD30/TNFRSF8, gp130/sIL6RB, IL32) decreased. The mechanisms responsible for immune cells-induced lowering of soluble mediators produced in response to SARS-CoV-2 infection need further analysis.

IL-27 has been proposed as an early biomarker of COVID-19 severity (Tamayo-Velasco et al., 2021). The ability of immune cells to dampen IL-27 production may suggest a possible role in reducing lung damage. On the other way, IL-27, as well as IL-34 levels, may affect the innate immune response, as shown by the negative correlation with NK-bright cells. Accordingly, in a previous work in patients with COVID-19, we demonstrated that the increase of inflammatory mediators was correlated with a reduction of innate and adaptive cytotoxic antiviral function (Bordoni et al., 2020).

The wide immunoprofiling analysis performed in this study highlights the pivotal role of immune-regulatory mediators in shaping the immune response. IL-27 and IL-35 (together with TGFβ and IL-10) are the most extensively studied cytokines in tissues such as the lung (Branchett and Lloyd, 2019). IL-35 can inhibit T cell proliferation and cytotoxicity and reduce T cell activation. Moreover, IL-35 was found to increase in both lungs of mice and serum of humans following influenza infection, and its expression was further enhanced in influenza-infected mice following secondary pneumococcal infection (Chen et al., 2016). The main role of IL-27 in respiratory infection has been proposed. In influenza infection, the delivery of recombinant IL-27 limited the recruitment of inflammatory monocytes, neutrophils, and NK cells into the lung, without affecting the T cell response, suggesting that IL-27 can control the immune response to influenza (Liu et al., 2014). IL-34 plays diverse roles in diseases, owing to its inflammatory and immunosuppressive properties. Elevated IL-34 expression has been observed in lung cancers and pulmonary infections, although its role is not well defined (Baghdadi et al., 2018; Zhou et al., 2018). γδ T cells frequency was reduced in SARS-CoV-2-infected HAE co-cultures and negatively correlated with IL-35. Accordingly, a decrease of γδ T cell has been observed in patients with severe COVID-19 (Carissimo et al., 2020; Lei et al., 2020), and a possible protective role has also been proposed in SARS-CoV infection (Poccia et al., 2006).

Interestingly the analysis of enrichment pathway resulting from 36 soluble mediators associated with different immune cell subsets, revealed that the RIG-I pathway (a key activator of type I interferon (IFN)

antiviral signaling) was enriched in infected HAE-PBMC and correlated to CD8 T cells. Notably, a high concentration of RIG-I is found around tight junctions, suggesting that they could act as apical foci for antiviral sensors (Mukherjee et al., 2009).

Altogether, we described a strict interplay between immunoregulatory/inflammatory signals (e.g., IL-35, IL-27, and IL-34) induced by SARS-CoV-2 infection and innate and adaptive immune cells that can be useful to develop novel therapeutic strategies aimed at promoting effective immune responses against respiratory viruses.

Limitations of the study

A major limitation of this work, as for all the *in vitro* model of infection, is that the airway epithelial and immune cell co-culture system described in this study likely does not reflect the dynamic interaction of infiltrating immune cells within the airway at different stages of SARS-CoV-2 infection. Nevertheless, this experimental approach may allow to dissect epithelial-immune cell cross-talk during SARS-CoV-2 infection, and to identify possible key pathogenic/protective processes that should be subsequently validated in an *in vivo* animal model.

STAR★METHODS

Detailed methods are provided in the online version of this paper and include the following:

- KEY RESOURCES TABLE
- RESOURCE AVAILABILITY
  - Lead contact
  - Materials availability
  - Data and code availability
- EXPERIMENTAL MODEL AND SUBJECT DETAILS
  - Human subjects
  - Human primary bronchial epithelial cells
  - Vero E6 cell line
- METHOD DETAILS
  - SARS-CoV-2 infection of HAE
  - Flow cytometry staining and analysis
  - Real time RT-PCR
  - Viral quantification and titration
  - Multiplex microbead-based immunoassay
  - Immunofluorescence
  - Protein network and pathways analysis
- QUANTIFICATION AND STATISTICAL ANALYSIS

SUPPLEMENTAL INFORMATION

Supplemental information can be found online at https://doi.org/10.1016/j.isci.2022.103854.

ACKNOWLEDGMENTS

This work was supported by Ministero della Salute (Ricerca Corrente Linea one; COVID-2020-12371735 – available at URL: https://www.salute.gov.it/) and by Fondazione Roma and Valentino (generous liberal donations funding COVID-19 research – available at https://www.inmi.it/?s=fondazione+roma). The authors thank Andrea Passavanti Pizzuto for your help in bioinformatic analysis.

AUTHOR CONTRIBUTIONS

Conceptualization, C.A.; Data curation, V.B., G.M., D.M., M.A.; Formal analysis, V.B., G.M., D.M., M.A, G.M.F. and C.A.; Funding acquisition, G.I. and C.A.; Investigation, V.B., G.M., D.M., A.S., C.C., and C.A.; Methodology, E.C., E.T., R.C., G.G., S.T.; Supervision, G.M.F., M.R.C. and C.A.; Writing—original draft, V.B., G.M. D.M., M.A.,; Writing—review and editing, C.A. All authors have read and agreed to the published version of the article.

DECLARATION OF INTERESTS

The authors declare no competing interests.

Received: November 19, 2021
Revised: December 21, 2021
Accepted: January 27, 2022
Published: February 18, 2022

REFERENCES

Baghdadi, M., Endo, H., Takano, A., Ishikawa, K., Kameda, Y., Wada, H., Miyagi, Y., Yokose, T., Ito, H., Nakayama, H., et al. (2018). High co-expression of IL-34 and M-CSF correlates with tumor progression and poor survival in lung cancers. Sci. Rep. *8*, 418. https://doi.org/10.1038/s41598-017-18796-8.

Blanco-Melo, D., Nilsson-Payant, B.E., Liu, W.C., Uhl, S., Hoagland, D., Moller, R., Jordan, T.X., Oishi, K., panis, M., Sachs, D., et al. (2020). Imbalanced host response to SARS-CoV-2 drives development of COVID-19. Cell *181*, 1036–1045.e9. https://doi.org/10.1016/j.cell.2020.04.026.

Bordoni, V., Sacchi, A., Cimini, E., Notari, S., Grassi, G., Tartaglia, E., Casetti, R., Giancola, M.L., Bevilacqua, N., Maeurer, M., et al. (2020). An inflammatory profile correlates with decreased frequency of cytotoxic cells in coronavirus disease 2019. Clin. Infect. Dis. *71*, 2272–2275. https://doi.org/10.1093/cid/ciaa577.

Branchett, W.J., and Lloyd, C.M. (2019). Regulatory cytokine function in the respiratory tract. Mucosal Immunol. *12*, 589–600. https://doi.org/10.1038/s41385-019-0158-0.

Carissimo, G., Xu, W., Kwok, I., Abdad, M.Y., Chan, Y.H., Fong, S.W., Puan, K.J., Lee, C.Y.P., Yeo, N.K.W., Amrun, S.N., et al. (2020). Whole blood immunophenotyping uncovers immature neutrophil-to-VD2 T-cell ratio as an early marker for severe COVID-19. Nat. Commun. *11*. 5243-020-19080-6. https://doi.org/10.1038/s41467-020-19080-6.

Chen, Y., Wang, C.J., Lin, S.H., Zhang, M., Li, S.Y., and Xu, F. (2016). Interleukin-35 is upregulated in response to influenza virus infection and secondary bacterial pneumonia. Cytokine *81*, 23–27. https://doi.org/10.1016/j.cyto.2016.01.016.

Chua, R.L., Lukassen, S., Trump, S., Hennig, B.P., Wendisch, D., Pott, F., Debnath, O., Thürmann, L., Kurth, F., Volker, M.T., et al. (2020). COVID-19 severity correlates with airway epithelium-immune cell interactions identified by single-cell analysis. Nat. Biotechnol. *38*, 970–979. https://doi.org/10.1038/s41587-020-0602-4.

Guan, W.J., Ni, Z.Y., Hu, Y., Liang, W.H., Ou, C.Q., He, J.X., Liu, L., Shan, H., Lei, C.L., Hui, D.S.C., et al. (2020). Clinical characteristics of coronavirus disease 2019 in China. N. Engl. J. Med. *382*, 1708–1720. https://doi.org/10.1056/NEJMoa2002032.

Hadjadj, J., Yatim, N., Barnabei, L., Corneau, A., Boussier, J., Smith, N., Péré, H., Charbit, B., Bondet, V., Chenevier-Gobeaux, C., et al. (2020). Impaired type I interferon activity and inflammatory responses in severe COVID-19 patients. Science *369*, 718–724. https://doi.org/10.1126/science.abc6027.

Hao, S., Ning, K., Kuz, C.A., Vorhies, K., Yan, Z., and Qiu, J. (2020). Long-term modeling of SARS-CoV-2 infection of in vitro cultured polarized human airway epithelium. mBio *11*. https://doi.org/10.1128/mBio.02852-20.

Hoffmann, M., Kleine-Weber, H., Schroeder, S., Kruger, N., Herrler, T., Erichsen, S., Schiergens, T.S., Herrler, G., Wu, N.H., Nitsche, A., et al. (2020). SARS-CoV-2 cell entry depends on ACE2 and TMPRSS2 and is blocked by a clinically proven protease inhibitor. Cell *181*, 271–280.e8. https://doi.org/10.1016/j.cell.2020.02.052.

Huang, C., Wang, Y., Li, X., Ren, L., Zhao, J., Hu, Y., Zhang, L., Fan, G., Xu, J., Gu, X., et al. (2020). Clinical features of patients infected with 2019 novel coronavirus in Wuhan, China. Lancet *395*, 497–506. https://doi.org/10.1016/S0140-6736(20)30183-5.

Lei, L., Qian, H., Yang, X., Zhang, X., Zhang, D., Dai, T., Guo, R., Shi, L., Cheng, Y., Zhang, B., et al. (2020). The phenotypic changes of gammadelta T cells in COVID-19 patients. J. Cell Mol. Med. *24*, 11603–11606. https://doi.org/10.1111/jcmm.15620.

Liao, M., Liu, Y., Yuan, J., Wen, Y., Xu, G., Zhao, J., Cheng, L., Li, J., Wang, X., Wang, F., et al. (2020). Single-cell landscape of bronchoalveolar immune cells in patients with COVID-19. Nat. Med. *26*, 842–844. https://doi.org/10.1038/s41591-020-0901-9.

Liu, F.D., Kenngott, E.E., Schroter, M.F., Kuhl, A., Jennrich, S., Watzlawick, R., Hoffmann, U., Wolff, T., Norley, S., Sheffold, A., et al. (2014). Timed action of IL-27 protects from immunopathology while preserving defense in influenza. PLoS Pathog. *10*, e1004110. https://doi.org/10.1371/journal.ppat.1004110.

McNamara, P.S., Fonceca, A.M., Howarth, D., Correia, J.B., Slupsky, J.R., Trinick, R.E., Al Turaiki, W., Smyth, R.L., and Flanagan, B.F. (2013). Respiratory syncytial virus infection of airway epithelial cells, in vivo and in vitro, supports pulmonary antibody responses by inducing expression of the B cell differentiation factor BAFF. Thorax *68*, 76–81. https://doi.org/10.1136/thoraxjnl-2012-202288.

Mehta, P., McAuley, D.F., Brown, M., Sanchez, E., Tattersall, R.S., and Manson, J.J. (2020). COVID-19: consider cytokine storm syndromes and immunosuppression. Lancet *395*, 1033–1034. https://doi.org/10.1016/S0140-6736(20)30628-0.

Mukherjee, A., Morosky, S.A., Shen, L., Weber, C.R., Turner, J.R., Kim, K.S., Wang, T., Coyne, C.B., et al. (2009). Retinoic acid-induced gene-1 (RIG-I) associates with the actin cytoskeleton via caspase activation and recruitment domain-dependent interactions. J. Biol. Chem. *284*, 6486–6494. https://doi.org/10.1074/jbc.M807547200.

Nawijn, M.C., and Timens, W. (2020). Can ACE2 expression explain SARS-CoV-2 infection of the respiratory epithelia in COVID-19? Mol. Syst. Biol. *16*, e9841. https://doi.org/10.15252/msb.20209841.

Onabajo, O.O., Banday, A.R., Stanifer, M.L., Yan, W., Obajemu, A., Santer, D.M., Florez-Vargas, O., Piontkivska, H., Vargas, J.M., Ring, T.J., et al. (2020). Interferons and viruses induce a novel truncated ACE2 isoform and not the full-length SARS-CoV-2 receptor. Nat. Genet. *52*, 1283–1293. https://doi.org/10.1038/s41588-020-00731-9.

Pizzorno, A., Padey, B., Julien, T., Trouillet-Assant, S., Traversier, A., Errazuriz-Cerda, E., Fouret, J., Dubois, J., Gaymard, A., Lescure, F.X., et al. (2020). Characterization and treatment of SARS-CoV-2 in nasal and bronchial human airway epithelia. Cell Rep. Med. *1*, 100059. https://doi.org/10.1016/j.xcrm.2020.100059.

Poccia, F., Agrati, C., Castilletti, C., Bordi, L., Gioia, C., Horejsh, D., Ippolito, G., Chan, P.K.S., Hui, D.S.C., Sung, J.J.Y., et al. (2006). Anti-severe acute respiratory syndrome coronavirus immune responses: the role played by V gamma 9V delta 2 T cells. J. Infect. Dis. *193*, 1244–1249. https://doi.org/10.1086/502975.

Ravindra, N.G., Alfajaro, M.M., Gasque, V., Huston, N.C., Wan, H., Szigeti-Buck, K., Yasumoto, Y., Greaney, A.M., Habet, V., Chow, R.D., et al. (2021). Single-cell longitudinal analysis of SARS-CoV-2 infection in human airway epithelium identifies target cells, alterations in gene expression, and cell state changes. PLoS Biol. *19*, e3001143. https://doi.org/10.1371/journal.pbio.3001143.

Song, J.W., Zhang, C., Fan, X., Meng, F.P., Xu, Z., Xia, P., Cao, W.J., Yang, T., Dai, X.P., Wang, S.Y., et al. (2020). Immunological and inflammatory profiles in mild and severe cases of COVID-19. Nat. Commun. *11*. 3410-020-17240-2. https://doi.org/10.1038/s41467-020-17240-2.

Tamayo-Velasco, A., Martinez-Paz, P., Penarrubia-Ponce, M.J., De la Fuente, I., Perez-Gonzalez, S., Fernandez, I., Dueñas, C., Gómez-Sánchez, E., Lorenzo-López, M., Gómez-Pesquera, E., et al. (2021). HGF, IL-1alpha, and IL-27 are robust biomarkers in early severity stratification of COVID-19 patients. J. Clin. Med *10*. https://doi.org/10.3390/jcm10092017.

Tian, S., Xiong, Y., Liu, H., Niu, L., Guo, J., Liao, M., and Xiao, S.Y. (2020). Pathological study of the 2019 novel coronavirus disease (COVID-19) through postmortem core biopsies. Mod. Pathol.

33, 1007–1014. https://doi.org/10.1038/s41379-020-0536-x.

Xu, Z., Shi, L., Wang, Y., Zhang, J., Huang, L., Zhang, C., Liu, S., Zhao, P., Liu, H., Zhu, L., et al. (2020). Pathological findings of COVID-19 associated with acute respiratory distress syndrome. Lancet Respir. Med. *8*, 420–422.

Zhou, F., Yu, T., Du, R., Fan, G., Liu, Y., Liu, Z., Xiang, J., Wang, Y., Song, B., Gu, X., et al. (2020). Clinical course and risk factors for mortality of adult inpatients with COVID-19 in Wuhan, China: a retrospective cohort study. Lancet *395*, 1054–1062. https://doi.org/10.1016/S0140-6736(20)30566-3.

Zhou, J., Sun, X., Zhang, J., Yang, Y., Chen, D., and Cao, J. (2018). IL-34 regulates IL-6 and IL-8 production in human lung fibroblasts via MAPK, PI3K-Akt, JAK and NF-kappaB signaling pathways. Int. Immunopharmacol. *61*, 119–125. https://doi.org/10.1016/j.intimp.2018.05.023.

Zhu, N., Wang, W., Liu, Z., Liang, C., Wang, W., Ye, F., Huang, B., Zhao, L., Wang, H., Zhou, W., et al. (2020a). Morphogenesis and cytopathic effect of SARS-CoV-2 infection in human airway epithelial cells. Nat. Commun. *11*. 3910-020-17796-z. https://doi.org/10.1038/s41467-020-17796-z.

Zhu, N., Zhang, D., Wang, W., Li, X., Yang, B., Song, J., Zhao, X., Huang, B., Shi, W., Lu, R., et al. (2020b). A novel coronavirus from patients with pneumonia in China, 2019. N. Engl. J. Med. *382*, 727–733. https://doi.org/10.1056/NEJMoa2001017.

STAR★METHODS

KEY RESOURCES TABLE

REAGENT or RESOURCE	SOURCE	IDENTIFIER
Antibodies		
Mouse anti-human CD3 PerCP-Cy5.5 (Clone SP34-2)	BD Biosciences	Cat.#552852; RRID: AB_394493
Mouse Anti-Human CD56 APC (Clone B159)	BD Biosciences	Cat.#555518; RRID: AB_398601
Mouse Anti-Human CD16 PE-Cy^{TM}7 (Clone 3G8)	BD Biosciences	Cat.#557744; RRID: AB_396850
Mouse Anti-Human CD4 FITC (Clone RPA-T4)	BD Biosciences	Cat.#555346; RRID: AB_395751
Mouse Anti-Human CD8 PE (Clone RPA-T8)	BD Biosciences	Cat.#555367; RRID: AB_395770
Mouse Anti-Human CD14 APC-H7 (Clone MφP9)	BD Biosciences	Cat.#641394;RRID:AB_1645725
Mouse Anti-Human CD16 V450 (Clone 3G8)	BD Biosciences	Cat.#560475; RRID: AB_1645561
Mouse Anti-Human CD45 Krome Orange (Clone J33)	Beckman Coulter	Cat.#B36294;RRID:AB_2833027
Mouse Anti-Human Vδ2 Brilliant Violet 605 (Clone B6)	Biolegend	Cat.#331430;RRID:AB_2783212
Rabbit Polyclonal Antibody anti-ZO-1	Thermo Fisher Scientific	Cat.#40-2200; RRID:AB_2533456
Mouse monoclonal Antibody anti-SARS-CoV-2 spike antibody (Clone 1A9)	GeneTex	Cat.#GTX632604; RRID:AB_2864418
goat Anti-Mouse IgG1 (γ1), CF 488A	Sigma Aldrich	Cat.#SAB4600238
goat Anti-Rabbit IgG, CF 647	Sigma Aldrich	Cat.#SAB4600352
Bacterial and virus strains		
Human 2019-nCoV strain 2019-nCoV/Italy-INMI1, clade V	EVAg Portal	Ref-SKU: 008V-03893
Biological samples		
Peripheral blood Mononuclear cells from healthy donors	Recruited at INMI L.Spallanzani (Ethical approvement: 70/2018)	N/A
Critical commercial assays		
Bio-Plex Pro Human Inflammation Panel 1, 37-Plex	Bio-Rad	Cat.#171AL001M
Direct-zol RNA MicroPrep KIT	Zymo Research	Cat.#R1051
AMV-reverse transcriptase	Promega	Cat.#M5108
Qiamp viral RNA kit	Qiagen	Cat.#52904
RealStar SARS-CoV-2 RT-PCR Kit	Altona Diagnostics	Cat.#821005
FastStart Essential DNA Green Master	Roche	Cat.#06402712001
Experimental models: Cell lines		
Human adult Bronchial Epithelial Cells (HBEpCs)	Cell Applications	Cat.#502–05a
Cercopithecus aethiops Vero E6 Cells	ATCC	CRL-1586
Oligonucleotides		
See Table S1: Oligonucleotides	This paper	N/A

(*Continued on next page*)

Continued

REAGENT or RESOURCE	SOURCE	IDENTIFIER
Software and algorithms		
RStudio	The R Foundation	http://www.rstudio.org
GraphPad Prism 8	GraphPad	https://www.graphpad.com/
Cytoscape 3.8.2	National Resource for Network Biology	https://cytoscape.org/
BD FACSuite software	BD Biosciences	https://www.bdbiosciences.com/
Leica Application Software (LAS) X 3.7.2	Leica Microsystems	https://www.leica-microsystems.com/

RESOURCE AVAILABILITY

Lead contact

Further information and requests for reagents may be directed to and will be fulfilled by the lead contact, Chiara Agrati (chiara.agrati@inmi.it).

Materials availability

This Study did not generate new unique reagents.

Data and code availability

- The data presented in this study are openly available at http://rawdata.inmi.it.
- This paper does not report original code. All code utilized in the paper is available online and listed in the key resources table.
- Any additional information required to re-analyze the data reported in this paper is available from the lead contact upon request.

EXPERIMENTAL MODEL AND SUBJECT DETAILS

Human subjects

The immune cells from residual samples obtained for diagnostic purpose of healthy donors were isolated in compliance with the principles included in the Declaration of Helsinki. The Ethics Committee of the INMI L Spallanzani approved the study protocol (Ethical approvement: 70/2018). PBMCs from four different healthy donors (age: 46, 51, 53, 36; negative for SARS-CoV-2 molecular and serological tests) were isolated from whole blood by density gradient centrifugation (Lympholyte-H; Cedarlane Labs). PBMCs were suspended in RPMI 1640 (Corning Incorporated) supplemented with 2 mM L-glutamine, 50 U/mL penicillin, and 50 μg/mL streptomycin.

Human primary bronchial epithelial cells

Human primary adult Bronchial Epithelial Cells (lot 2463, HBEpCs, Cell Applications) were thawed in Bronchial/Tracheal Epithelial growth medium (Cell Applications), expanded and frozen in single aliquots for further experiments. After 3–5 days, cells were detached using the Animal Component-Free (ACF) Cell Dissociation Kit (STEMCELL Technologies) and seeded in 12 mm transwell inserts (STEMCELL Technologies) in PneumaCult Ex Plus Medium (STEMCELL, Technologies), supplemented with 2 mM L-glutamine (Corning Incorporated, Corning, New York, USA), 50 U/mL penicillin, and 50 μg/mL streptomycin (Corning Incorporated), at the density of 1.1 × 10^5 cells/mL in a humidified atmosphere (5% CO2) at 37°C. At the confluence, the medium was cleared from both apical and basal sides and PneumaCult-ALI-S Medium (STEMCELL Technologies) was only added in the lower chamber, leaving the apical chamber in contact with the air and inducing the differentiation for 21 days. The medium was changed every two days until complete differentiation, observable from mucus production, which can be removed using 0.5 mL of Phosphate buffered saline 1× (PBS). The well differentiated human airway epithelium (HAE) was therefore used for successive experiments. The cell viability was verified overtime checking the structural epithelial architecture by immunofluorescence analysis.

Vero E6 cell line

Vero E6 cells (ATCC® CRL-1586) were culture in Eagle's Minimum Essential Medium (MEM, Sigma-Aldrich St. Louis, Missouri, USA) supplemented with 2 mM L-glutamine, 50 U/mL penicillin, and 50 μg/mL streptomycin, and 10% Foetal Bovine Se-rum (FBS, GIBCO).

METHOD DETAILS

SARS-CoV-2 infection of HAE

HAE cells were infected with SARS-CoV-2, (Human 2019-nCoV strain 2019-nCoV/Italy-INMI1, clade V; Ref-SKU: 008V-03893 European Virus Archive – GLOB-AL, GISAID: BetaCoV/Italy/INMI1-isl/2020: EPI_ISL_410545) in MEM at a multiplicity of infection (M.O.I.) of 0.1. Viral inoculum or medium only (not infected) was applied on the apical side and cells were incubated for 1 h and 30′ at 37°C, 5% CO2. Viral inoculum was then removed and cells washed with 0.3 mL of 1×PBS two times. Next, 1 mL of RPMI 1640 with 5 % Human Serum (Sigma Aldrich) was added to the basal chamber of each well and cells were cultured at 37°C, 5% CO2. In co-culture experiments (HAE-PBMC), two million of PBMCs were plated in the basal chamber. Soon after inoculum removal and at two- and six-days post infection, we collected HAE cells, PBMCs, and basal supernatant. All the analysis were performed in 4 independent experiments in biological duplicates. Moreover, at the time of collection transwell inserts were transferred into a clean plate, 1xPBS was added to the apical chamber and after 15 min at 37°C, 5% CO2, PBS was collected and stored (apical supernatant).

Flow cytometry staining and analysis

NK, T and Monocyte cell surface antigens were analysed by flow cytometry. Briefly, two million PBMCs were stained with a surface antibody's cocktail: anti-CD3 PerCP-Cy 5.5, anti-CD56 APC and anti-CD16 PE-CyTM7 from BD Biosciences, anti-CD45 Krome Orange from Beckman Coulter and anti-Vδ2 Brilliant Violet 605 from Biolegend (Mix NK and gammadelta T cells); anti-CD4 FITC, anti-CD8 PE and anti-CD3 Pacific Blue from BD Biosciences and anti-CD45 Krome Orange (Mix T cells); anti-CD14 APC-H7 and anti-CD16 V450 from BD Biosciences and anti-CD45 Krome Orange (Mix Monocytes), in 1× PBS, 1% Bovine Serum Albumin (BSA) (from Sigma Aldrich) and 0.1% Sodium azide (NaN3) (from Serva) solution for 15 min at 4°C. Afterwards, PBMCs were washed with 0.3 mL of 1× PBS, 1% BSA and 0.1% NaN3 solution and centrifuged at 1600 rpm for 5 min. Next, PBMCs were fixed with 1% Paraformaldehyde (PFA) (Bio-Rad, Hercules, California, USA) in 1× PBS, 1% BSA and 0.1% NaN3 solution for 15 min at room temperature in the dark, washed as before and centrifuged at 1600 rpm for 5 min. Cells were acquired using a FACSLyric (BD Biosciences) and analysed by BD FACSuite software (BD Biosciences).

Real time RT-PCR

Total RNA was extracted from HAE culture using Direct-zol RNA MicroPrep KIT (Zymo Research Corp.) according to the manufacturer's instructions. For RT-PCR analyses, single-stranded cDNA was obtained by reverse transcription of 1 μg of total RNA using AMV-reverse transcriptase (Promega Corporation). For cellular gene expression analysis, ISG15, ISG56, INFα, INFβ, ACE2, truncated_ACE2 and TMPRSS2 mRNA were analysed by quantitative PCR using the following primers purchased from Sigma-Aldrich: ISG15 forward: 5′-GCAGATCACCCAGAAGATCG-3′, reverse: 5′-GGCCCTTGTTATTCCTCACC-3′; ISG56 forward: 5′-CCTTGCTGAAGTGTGGAGGA-3′, reverse: 5′-CCAGGCGATAGGCAGAGA-3′; INF-α forward: 5′-TGGGCTGTGATCTGCCTCAAAC-3′, reverse: 5′-CAGCCTTTTGGAACTGGTTGCC-3′; INF-β forward: 5′-CTTGGATTCCTACAAAGAAGCAGC-3′, reverse: 5′-TCCTCCTTCTGGAACTGCTGCA-3′; ACE2 forward: 5′-GGGCGACTTCAGGATCCTTAT-3′, reverse: 5′-GGATATGCCCCATCTCATGATG-3′; truncated_ACE2 forward: 5′-GGAAGCAGGCTGGGACAAA-3′, reverse: 5′-AGCTGTCAGGAAGTCGTCCATT-3′; TMPRSS2 forward: 5′-GTCCCCACTGTCTACGAGGT-3′, reverse: 5′-CAGACGACGGGGTTGGAAG-3′. qPCR was performed with FastStart Essential DNA Green Master (Roche) according to the manufacturer's instructions. The expression levels were normalized to GAPDH level (GAPDH forward: 5′-GGTGG TCTCCTCTGACTTCAACA-3′, reverse: 5′-GTGGTCGTTGAGGGCAATG-3′) using the equation "2−ΔCt". All qPCR reactions were performed in a Corbett 212 Rotor-gene6000 Real-Time PCR System.

Viral quantification and titration

RNA from 140 μL of HAE culture supernatant was extracted using the Qiamp viral RNA kit (Qiagen), following manufacturers instruction and eluted in 50 μL of elution buffer.

For viral replication determination, Real time RT- PCR was performed on 10 µL of RNA extracted from supernatant, or 40 ng of cell-associated RNA using the RealStar® SARS-CoV-2 RT-PCR Kit RUO (Altona Diagnostics), which amplifies the E— and S- viral genes.

To estimate the production of infectious SARS-CoV-2, serial dilution of HAE cell supernatants were put in contact with sub-confluent VeroE6 cells seeded in 96-well plates in MEM containing 2% FBS. At day 5 after infection, cells were observed for cytopathic effect CPE and TCID50/mL was measured and analysed by Reed-Muench method.

Multiplex microbead-based immunoassay

The inflammation factor levels were analysed using a Bio-Plex Pro™ Human Inflammation Panel 1, 37-Plex (#171AL001M, Bio-Rad) according to the manufacturer's instructions. 0.05 mL of each collected supernatant, at six days after infection, were used for the assay. The lecture of the plate was performed with BioPlex® MAGPIX Multiplex Reader.

Immunofluorescence

Transwells after six days from the infection were fixed in PAF 4% diluted in PBS 1× for 20 min at RT. The transwells were cut with a sterile scalpel and laid down in a new 24 cell culture well plate with the side cells located face-up. Then, transwells were washed with PBS 1× three times for five min each and blocked with Blocking Buffer (2% Goat Serum from Invitrogen; 1% BSA from Sigma Aldrich; 0.1% Fish Gelatin Blocking Agent from Biotium; 0.1% Triton X-100 and 0.05% Tween20 from Sigma Aldrich in 1×PBS) for 1 hone hour at RT. Later, blocking buffer was removed, transwells were washed as before, 0.45 mL of primary antibodies (anti-ZO1 from Invitrogen; anti-SARS-CoV-2 spike antibody from GeneTex; in Primary Antibody Buffer (1% BSA and 0.1% Fish Gelatin Blocking Agent in 1×PBS) were added to each transwell and incubated overnight at 4°C in the dark. The following day primary antibodies were removed, transwells were washed as before, 0.45 mL of secondary antibodies (anti-Mouse IgG1 AF488 and anti-Rabbit IgG Alexa-647 from Sigma Aldrich) diluted 1:1000 in Secondary Antibody Buffer (1× PBS) were added to each transwell and incubated for 2 htwo hours at RT in the dark. Afterwards, secondary antibodies were removed, transwells were washed as before and membrane cell was mounted side up on slide using one drop of SlowFade Gold Antifade Mountant with DAPI (from Invitrogen). Therefore the images were acquired using a Leica THUNDER 3D Live Cell Imaging system (Leica Application Software (LAS) X 3.7.2; Leica Microsystems) using THUNDER Computational Clearing Settings at 63X magnification.

Protein network and pathways analysis

Cystoscape software (3.8.2 version) and STRING App were used to build protein-protein network using a 0,4 as confidence cutoff. STRING Enrichment analysis was performed to retrieve human KEGG pathways associated with different lymphomonocytes subset; redundant terms were filtered with 0,5 cutoff. RStudio software was used to build a bubble plot using ggplot2-based visualization.

QUANTIFICATION AND STATISTICAL ANALYSIS

Principal component analysis (PCA) was performed in order to identify the relevant information and visualize major trends inherent to the immunological profile. Data were analysed using RStudio software from http://www.rstudio.org with the libraries FactoMineR (for the analysis) and factoextra (for ggplot2-based visualization). To visualize a correlation matrix in R we used the corrplot function and generate a Heatmap object using correlation coefficients (computed using the Spearman) as input to the Heatmap. The heatmap was produced with the R package heatmap3. Quantitative variables were compared with nonparametric Wilcoxon test. Friedman along with Dunn's multiple comparisons test evaluated the statistical differences between more than two conditions. A p value lower than 0.05 was considered statistically significant. Statistical analyses were performed using GraphPad Prism v8.0 (GraphPad Software, Inc). More details of the statistical analysis are included in Figure legends.